J. Fluid Mech. (1997), *vol.* 330, *pp.* 339–347

Numerical calculations of the free-surface flow under a sluice gate

By J.-M. VANDEN-BROECK

Department of Mathematics and Center for the Mathematical Sciences, University of Wisconsin-Madison, WI 53706, USA

(Received 19 March 1996 and in revised form 11 July 1996)

The free-surface flow under a sluice gate is considered. The fluid is assumed to be inviscid and incompressible. The problem is solved numerically by using a boundary integral equation technique. Accurate numerical solutions are obtained when the intersection of the upstream free surface with the gate is a stagnation point. It is shown that the radiation condition is not satisfied far upstream and that there is a train of waves on the upstream free surface. For large values of the downstream Froude number F, the amplitude of the waves is so small that the upstream free surface is essentially flat. However for small values of F, the waves are of large amplitude. They ultimately approach the Stokes' limiting configuration with an angle of 120° at their crest as F is decreased.

1. Introduction

The free-surface flow under a sluice gate is a classical problem of fluid mechanics. A sketch of the flow configuration is shown in figure 1. It is a two-dimensional steady flow above an horizontal bottom. The flow is bounded above by two free surfaces AB and CD and a vertical wall BC. Far downstream there is a uniform flow with a constant velocity U and a constant depth H. As we shall see, the problem can be characterized by the downstream Froude number

$$F = \frac{U}{(gH)^{1/2}}. \tag{1.1}$$

Here g is the acceleration due to gravity.

Over the years, many analytical and numerical approximations have been obtained (see for example Binnie 1952; Benjamin 1956; Fangmeier & Strelkoff 1968; Larock 1969; Chung 1972). It is usually assumed that B is a stagnation point and that there is a uniform stream far upstream. The last assumption is the radiation condition which requires no waves far upstream. It is then possible to define an upstream Froude number

$$F_U = \frac{V}{(gD)^{1/2}}$$

where V and D are the constant velocity and depth far upstream. The Froude numbers F and F_U are related by the identity

$$F_U^2 = \frac{F^2}{8}\left[\left(\frac{8}{F^2}+1\right)^{1/2} - 1\right]^3 \tag{1.2}$$

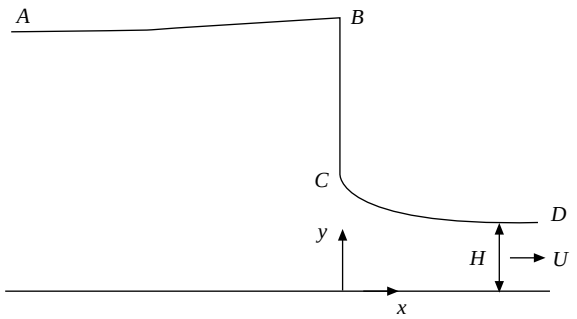

FIGURE 1. Sketch of the flow and of the coordinates.

(see Binnie 1952 for a derivation). The results obtained by using these approximations suggest that there is a one-parameter family of solutions and that the flow is subcritical upstream (i.e. $F_U < 1$) and supercritical downstream (i.e. $F > 1$).

In this paper we compute accurate numerical solutions for the fully nonlinear problem. The problem is first formulated as an integral equation for the unknown shapes of the free surfaces. This equation is then discretized and the resulting algebraic equations are solved by Newton's method. Such boundary integral methods were used before by Vanden-Broeck (1980), Forbes & Schwartz (1982), Vanden-Broeck & Dias (1992), Vanden-Broeck & Tuck (1994), Hocking & Vanden-Broeck (1996) and others. We also found that there is a one-parameter family of solutions. However our results show that the solutions do not satisfy the radiation condition: there is a train of waves on the upstream free surface. The amplitude of the waves comes as part of the solution. Our numerical findings indicate the non-existence of solutions which satisfy the radiation condition.

For $F > 2.4$, the waves are of very small amplitude and the upstream free surface is essentially flat. However for $F < 2.4$, the waves are quite noticeable and they ultimately become large nonlinear waves as F is decreased.

An interesting quantity is the contraction ratio

$$C_c = \frac{H}{y_C}. \tag{1.3}$$

Here y_C is the distance from the separation point C to the bottom. We show that our computed values of C_c are in good agreement with those of Fangmeier & Strelkoff (1968) for F large. This is consistent since the scheme of Fangmeier & Strelkoff neglects the waves upstream and our calculations show that the waves are indeed very small for F large.

The problem is formulated in §2. The numerical procedure is described in §3 and the results are discussed in §4.

2. Formulation

We consider the flow under a sluice gate. The fluid is assumed to be inviscid and incompressible and the flow to be irrotational. The flow domain is bounded below by an horizontal bottom and above by the free surfaces AB and CD and the vertical wall BC (see figure 1). We introduce Cartesian coordinates with the origin on the bottom and the y-axis along the vertical wall. Gravity g is acting in the negative y-direction. Far downstream the flow approaches a uniform stream with constant

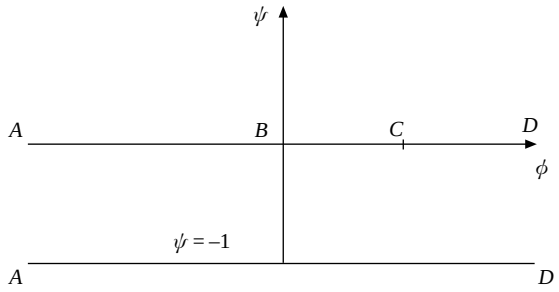

FIGURE 2. Flow configuration in the complex potential plane $f = \phi + \mathrm{i}\psi$.

velocity U and constant depth H. We define dimensionless variables by choosing H as the unit length and U as the unit velocity.

We introduce the complex potential function

$$f = \phi + \mathrm{i}\psi \tag{2.1}$$

and the complex velocity

$$w = u - \mathrm{i}v. \tag{2.2}$$

Here u and v are the horizontal and vertical components of the velocity. Following Benjamin (1956) and others, we assume that B is a stagnation point (i.e. $u = v = 0$ at B). Without loss of generality, we choose $\phi = 0$ at B and $\psi = 0$ on the streamline $ABCD$. It follows from our choice of dimensionless variables that $\psi = -1$ on the bottom. We denote by ϕ_c the value of ϕ at the separation point C. The flow configuration in the f-plane is sketched in figure 2.

In terms of the dimensionless variables, the dynamic boundary condition on the free surfaces AB and CD can be written as

$$u^2 + v^2 + \frac{2}{F^2}y = 1 + \frac{2}{F^2}. \tag{2.3}$$

Here F is the Froude number defined by (1.1).

The kinematic conditions on the bottom and on the gate BC imply

$$v = 0 \quad \text{on} \quad \psi = -1 \tag{2.4}$$

and

$$u = 0 \quad \text{on} \quad \psi = 0, \quad 0 < \phi < \phi_c. \tag{2.5}$$

This concludes the formulation of the problem. We seek w as an analytic function of f in the strip $-1 < \psi < 0$. This function must approach 1 as $\phi \to \infty$ and satisfy (2.3)–(2.5). As we shall see there is a one-parameter family of solutions. It is convenient to choose this parameter as ϕ_c.

We now reformulate the problem as an integral equation. First we define the function $\tau - \mathrm{i}\theta$ by

$$w = \mathrm{e}^{\tau - \mathrm{i}\theta} \tag{2.6}$$

and we map the flow domain onto the lower half of the ζ-plane by the transformation

$$\zeta = \alpha + \mathrm{i}\beta = \mathrm{e}^{\pi f}. \tag{2.7}$$

The flow in the ζ-plane is shown in figure 3.

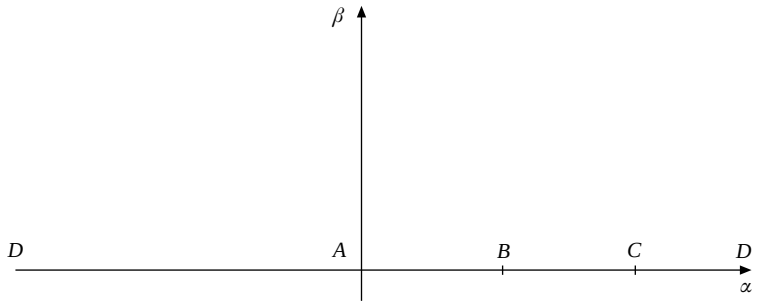

FIGURE 3. Flow configuration in the plane $\zeta = \alpha + \mathrm{i}\beta$.

Next we apply the Cauchy integral formula to the function $\tau - \mathrm{i}\theta$ in the complex ζ-plane. We choose a contour consisting of the real axis and a half-circle of arbitrary large radius in the lower half-plane. After taking the real part we obtain

$$\tau(\alpha) = \frac{1}{\pi}\int_{-\infty}^{\infty} \frac{\theta(\alpha')}{\alpha' - \alpha}\mathrm{d}\alpha'. \tag{2.8}$$

Here $\tau(\alpha)$ and $\theta(\alpha)$ denote the values of τ and θ on the axis $\beta = 0$. The integral in (2.8) is a Cauchy principal value. The kinematic conditions (2.4) and (2.5) imply

$$\theta(\alpha) = 0 \quad \text{for} \quad \alpha < 0 \tag{2.9}$$

and

$$\theta(\alpha) = -\pi/2 \quad \text{for} \quad 1 < \alpha < \alpha_c \tag{2.10}$$

where $\alpha_c = \mathrm{e}^{\pi\phi_c}$.

Substituting (2.9) and (2.10) into (2.8), we obtain

$$\tau(\alpha) = -\frac{1}{2}\ln\frac{|\alpha_c - \alpha|}{|1 - \alpha|} + \frac{1}{\pi}\int_0^1 \frac{\theta(\alpha')}{\alpha' - \alpha}\mathrm{d}\alpha' + \frac{1}{\pi}\int_{\alpha_c}^{\infty} \frac{\theta(\alpha')}{\alpha' - \alpha}\mathrm{d}\alpha'. \tag{2.11}$$

The equation (2.11) provides a relation between τ and θ on the free surfaces. We obtain another relation between τ and θ on the free surfaces in the following way. First we substitute (2.6) into (2.3). This yields

$$\mathrm{e}^{2\tau} + \frac{2}{F^2}y = 1 + \frac{2}{F^2}. \tag{2.12}$$

Next we evaluate the values of y on the free surfaces by using (2.7) and integrating the identity

$$\frac{\mathrm{d}(x + \mathrm{i}y)}{\mathrm{d}f} = w^{-1}. \tag{2.13}$$

This gives

$$y(\alpha) = 1 + \frac{F^2}{2} + \frac{1}{\pi}\int_1^{\alpha} \frac{\mathrm{e}^{-\tau(\alpha_o)}\sin\theta(\alpha_o)}{\alpha_o}\mathrm{d}\alpha_o \quad \text{for} \quad 0 < \alpha < 1 \tag{2.14}$$

and

$$y(\alpha) = 1 + \frac{1}{\pi}\int_{\infty}^{\alpha} \frac{\mathrm{e}^{-\tau(\alpha_o)}\sin\theta(\alpha_o)}{\alpha_o}\mathrm{d}\alpha_o \quad \text{for} \quad \alpha > \alpha_c. \tag{2.15}$$

Equations (2.11), (2.12), (2.14) and (2.15) define a nonlinear integral equation for the unknown function $\theta(\alpha)$ on the free surfaces $0 < \alpha < 1$ and $\alpha > \alpha_c$.

3. Numerical procedure

We solve the integral equation defined by (2.11), (2.12), (2.14) and (2.15) numerically. We use equally spaced points in the potential function ϕ. Thus we introduce the change of variables

$$\alpha = \mathrm{e}^{\pi\phi} \tag{3.1}$$

and rewrite (2.11) as

$$\tau'(\phi) = -\frac{1}{2}\ln\frac{|\alpha_c - \mathrm{e}^{\pi\phi}|}{|1 - \mathrm{e}^{\pi\phi}|} + \int_{-\infty}^{0} \frac{\theta'(\phi_o)\mathrm{e}^{\pi\phi_o}}{\mathrm{e}^{\pi\phi_o} - \mathrm{e}^{\pi\phi}}\mathrm{d}\phi_o + \int_{\phi_c}^{\infty} \frac{\theta'(\phi_o)\mathrm{e}^{\pi\phi_o}}{\mathrm{e}^{\pi\phi_o} - \mathrm{e}^{\pi\phi}}\mathrm{d}\phi_o. \tag{3.2}$$

Similarly we rewrite (2.14) and (2.15) as

$$y'(\phi) = 1 + \frac{F^2}{2} + \int_0^{\phi} \mathrm{e}^{-\tau'(\phi_o)} \sin\theta'(\phi_o)\mathrm{d}\phi_o, \tag{3.3a}$$

$$y'(\phi) = 1 + \int_{\infty}^{\phi} \mathrm{e}^{-\tau'(\phi_o)} \sin\theta'(\phi_o)\mathrm{d}\phi_o. \tag{3.3b}$$

Here $\tau'(\phi) = \tau(\mathrm{e}^{\pi\phi})$, $\theta'(\phi) = \theta(\mathrm{e}^{\pi\phi})$, etc.

Next we introduce the equally spaced mesh points

$$\phi_I^U = -(I-1)\Delta_1, \quad I = 1, \ldots, N_1 \tag{3.4}$$

and

$$\phi_I^D = \phi_c + (I-1)\Delta_2, \quad I = 1, \ldots, N_2 \tag{3.5}$$

on the upstream and downstream free surfaces. Here $\Delta_1 > 0$ and $\Delta_2 > 0$ are the mesh sizes. The corresponding unknowns are

$$\theta_I^U = \theta'(\phi_I^U), \quad I = 1, \ldots, N_1 \tag{3.6}$$

and

$$\theta_I^D = \theta'(\phi_I^D), \quad I = 1, \ldots, N_2. \tag{3.7}$$

Since $\theta_1^U = 0$ and $\theta_1^D = -\pi/2$, there are only $N_1 + N_2 - 2$ unknowns θ_I^U and θ_I^D.

We evaluate the values $\tau_{I+1/2}^U$ $\tau_{I+1/2}^D$ of $\tau'(\phi)$ at the midpoints

$$\phi_{I+1/2}^U = \frac{\phi_I^U + \phi_{I+1}^U}{2}, \quad I = 1, \ldots, N_1 - 1 \tag{3.8}$$

and

$$\phi_{I+1/2}^D = \frac{\phi_I^D + \phi_{I+1}^D}{2}, \quad I = 1, \ldots, N_2 - 1 \tag{3.9}$$

by applying the trapezoidal rule to the integrals in (3.2) with summations over the points ϕ_I^U and ϕ_I^D. The symmetry of the quadrature and of the distribution of mesh points enabled us to evaluate the Cauchy principal values as if they were ordinary integrals. In the calculations presented here, we follow Hocking & Vanden-Broeck (1996) and rewrite first the last integral in (3.2) as

$$\int_{\phi_c}^{\phi_{N_2}^D} \frac{(\theta'(\phi_0) - \theta_{I+1/2})\mathrm{e}^{\pi\phi_o}}{\mathrm{e}^{\pi\phi_o} - \mathrm{e}^{\pi\phi}}\mathrm{d}\phi_o + \frac{\theta_{I+1/2}}{\pi}\ln\frac{|\mathrm{e}^{\pi\phi_{N_2}^D} - \mathrm{e}^{\pi\phi}|}{|\alpha_c - \mathrm{e}^{\pi\phi}|} \tag{3.10}$$

before applying the trapezoidal rule. The values $\theta_{I+1/2}$ of θ at the mesh points (3.8)–(3.9) are evaluated in terms of the unknowns (3.6)–(3.7) by four-point interpolation formula.

Next we evaluate $y_I^U = y'(\phi_I^U)$ and $y_I^D = y'(\phi_I^D)$ by applying the trapezoidal rule to (3.3). This yields

$$y_1^U = 1 + \tfrac{1}{2}F^2,$$

$$y_I^U = y_{I-1}^U - e^{[-\tau_{I-1/2}^U]} \sin[\theta_{I-1/2}^U]\Delta_1, \quad I = 2, 3, \ldots, N_1;$$

$$y_{N_2}^D = 1,$$

$$y_I^D = y_{I+1}^D - e^{[-\tau_{I+1/2}^D]} \sin[\theta_{I+1/2}^D]\Delta_2, \quad I = N_2 - 1, N_2 - 2, \ldots, 1.$$

We use these values to evaluate $y'(\phi)$ at the midpoints (3.6) and (3.7) by interpolation formulas.

We now satisfy (2.12) at the midpoints (3.8) and (3.9). This yields $N_1 + N_2 - 2$ nonlinear algebraic equations for the $N_1 + N_2 - 1$ unknowns F, $\theta_I^U, I = 2, \ldots, N_1$ and $\theta_I^D, I = 2, \ldots, N_2$.

The last equation is obtained by fixing the length of the plate BC. Using (2.6), (2.10) and (2.13), we obtain

$$\frac{\partial y}{\partial \phi} = -e^{-\tau} \quad \text{on} \quad 0 < \phi < \phi_c \tag{3.11}$$

We use (3.2) to evaluate $\tau'(\phi)$ for $0 < \phi < \phi_c$ and integrate (3.11) numerically. This yields the length L of the plate BC in terms on the unknowns. The last equation is then

$$y_1^U - y_1^D - L = 0. \tag{3.12}$$

For a given value of ϕ_c, this system of $N_1 + N_2 - 1$ equations with $N_1 + N_2 - 1$ unknowns is solved by Newton's method.

4. Discussion of the results

We used the numerical scheme described in §3 to compute solutions for various values of ϕ_c.

Most of the calculations were performed with $N_1 = 320$, $N_2 = 360$, $\Delta_1 = 0.02$ and $\Delta_2 = 0.01$. We also calculated solutions with smaller values of Δ_1 and Δ_2 and larger values of N_1 and N_2 and checked that the results presented here are independent of these parameters within graphical accuracy. An example of such a check is presented at the end of this section.

Typical free-surface profiles are shown in figure 4(*a–e*). There is a train of waves on the upstream free surface. However, for large values of F (let us say $F > 2.4$), the waves are so small that they cannot be seen on the figures and the profiles are essentially flat far upstream (see figure 4*a* and 4*b*). However for $F < 2.4$, the waves are clearly noticeable on the profiles (see figure 4*c–e*). As F decreases, the waves become large amplitude nonlinear waves with broad troughs and sharp crests (see figure 4*e*). We expect that they ultimately reach the Stokes limiting configuration with a 120° angle at their crests as F is further decreased.

The profiles of figure 4 show that the mean elevation of the upstream free surface increases as F increases. Since the flux UH is normalized to 1, it follows that the mean velocity far upstream decreases as F increases (this is also consistent with (1.2) which is a valid approximation when the waves are of small amplitude). Therefore the phase velocity of the waves decreases as F increases. This explains why the wavelength of the waves increases as we move from figure 4(*c*) to figure 4(*e*).

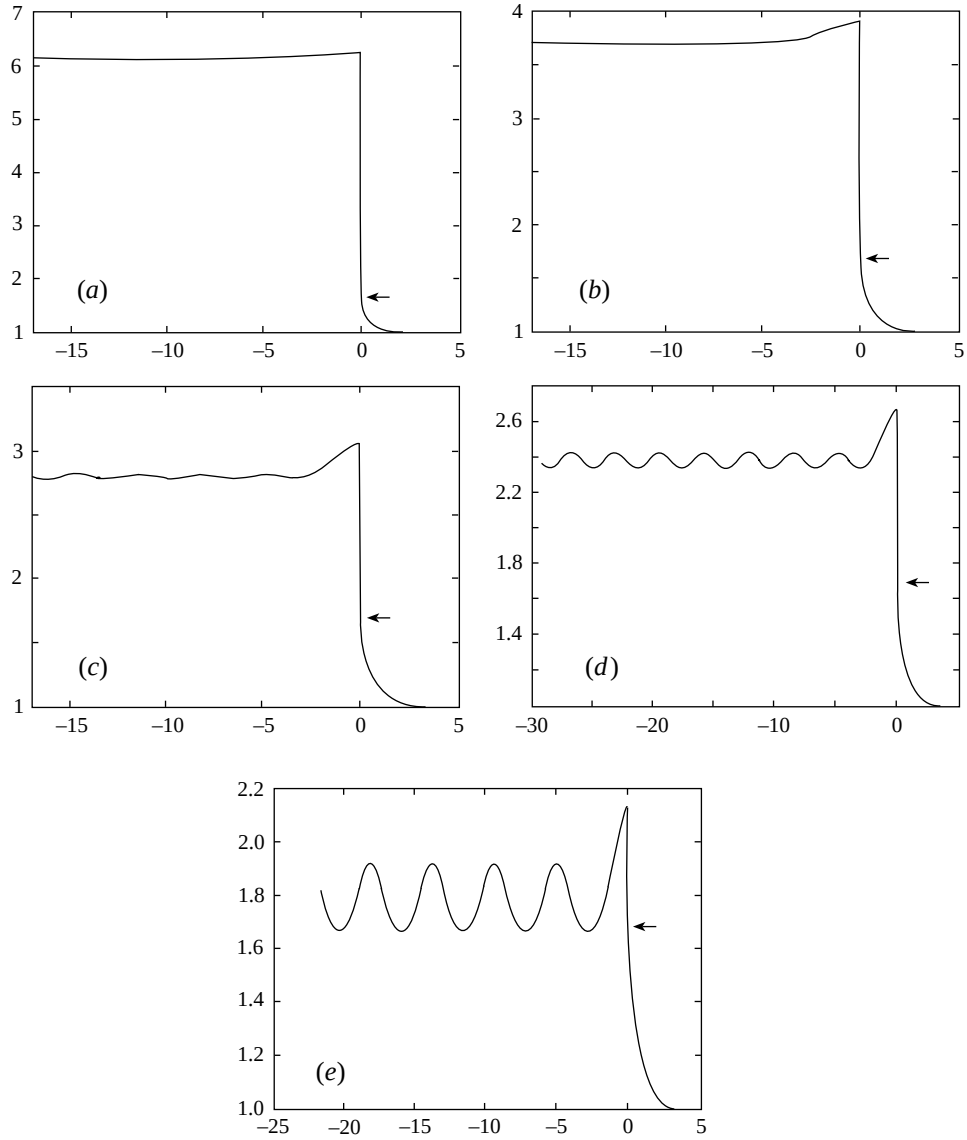

FIGURE 4. Computed profile of the free surfaces and of the gate. The arrow indicates the position of the point at which the downstream free surface separates from the gate. (*a*) $\phi_C = 0.71$ and $F = 3.25$; (*b*) $\phi_C = 0.41$ and $F = 2.41$; (*c*) $\phi_C = 0.26$ and $F = 2.03$; (*d*) $\phi_C = 0.19$ and $F = 1.83$; (*e*) $\phi_C = 0.075$ and $F = 1.51$.

In figure 5, we show values of the contraction ratio C_c (defined in (1.3)) versus y_C/y_B. Here y_C and y_B are the ordinates of the points C and B (see figure 1). As y_C/y_B approaches zero, $y_B \to \infty$ and $F \to \infty$. The problem reduces then to a classical free-streamline flow (Batchelor 1967, p. 495) and

$$C_c = \frac{\pi}{\pi + 2}. \tag{4.1}$$

The symbols in figure 5 are numerical values taken from the figure 13 in Fangmeier & Strelkoff (1968). These numerical values are in good agreement with ours for small

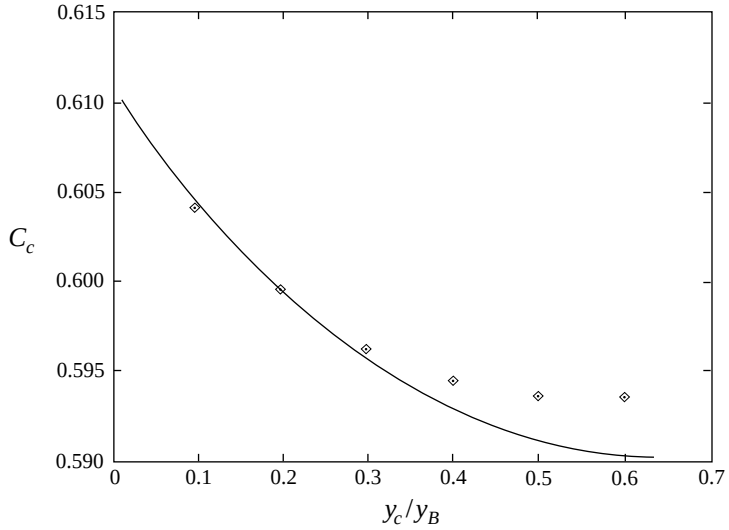

FIGURE 5. Values of the contraction coefficient C_c versus y_C/y_B. The symbols correspond to the calculations of Fangmeier & Strelkoff (1968).

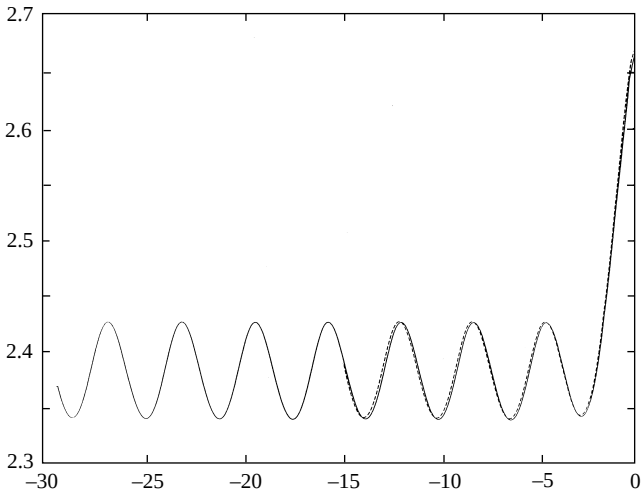

FIGURE 6. Computed profiles of the upstream free surface with $N_1 = 320$, $N_2 = 360$, $\Delta_1 = 0.04$ and $\Delta_2 = 0.01$ (solid curve) and $N_1 = 320$, $N_2 = 360$, $\Delta_1 = 0.02$ and $\Delta_2 = 0.01$ (broken line).

values of y_C/y_B (i.e. for large values of F). This is consistent since Fangmeier & Strelkoff assumed that there are no waves upstream and our results show that the waves are of very small amplitude for F large.

In figure 6, we present an example of the checks we used to test the accuracy of the numerical results. Both curves are computed upstream free surfaces for $\phi_C = 0.19$. Figure 6 shows that the results are independent of $\phi^U_{N_1}$.

The results presented in this section show that there is a train of waves on the upstream free surface. The amplitude of these waves is different from zero (except in the limit $F \to \infty$). This indicates the non-existence of solutions satisfying the radiation condition (which requires no waves far upstream). In particular the

numerical procedure of §3 diverges if we try to impose the radiation condition for example by forcing the free surface to be flat far upstream.

Finally let us mention that a well-posed mathematical problem is obtained by replacing the upstream free surface by a rigid lid. Accurate numerical solutions for this configuration were recently obtained by Asavanant & Vanden-Broeck (1996). Their predicted values of C_c are in good agreement with our values in figure 5 for y_C/y_B smaller than 0.3.

5. Conclusions

We have performed accurate numerical calculations for the free-surface flow under a sluice gate. We have shown that the usual assumption of a uniform stream upstream is incorrect and that there is a train of waves upstream. The amplitude of the waves is different from zero and no solutions satisfying the radiation condition were found. In the calculations presented here, we assumed that B is a stagnation point. We could have assumed instead that the upstream free surface is tangent to the gate at the separation point (the existence of such flow was demonstrated numerically by Asavanant & Vanden-Broeck 1996 for an inclined gate). An interesting question is whether or not there are waves under this assumption and work is progressing on this problem.

This work was supported in part by the National Science Foundation.

REFERENCES

Asavanant, J. & Vanden-Broeck, J.-M. 1996 Nonlinear free surface flows emerging from a vessel and flows under a sluice gate. *J. Austral. Math. Soc.* B **38**, 63–86.

Batchelor, G. K. 1967 *An Introduction to Fluid Dynamics*. Cambridge University Press.

Benjamin, B. 1956 On the flow in channels when rigid obstacles are placed in the stream. *J. Fluid Mech.* **1**, 227–248.

Binnie, A. M. 1952 The flow of water under a sluice gate. *Q. J. Mech. Appl. Maths* **5**, 395–407.

Chung, Y. K. 1972 Solution of flow under sluice gates. *ASCE J. Engng Mech. Div.* **98**, 121–140.

Fangmeier, D. D. & Strelkoff, T. S. 1968 Solution for gravity flow under a sluice gate. *ASCE J. Engng Mech. Div.* **94**, 153–176.

Forbes, L. K. & Schwartz, L. W. 1982 Free-surface flow over a semicircular obstruction. *J. Fluid Mech.* **114**, 299–314.

Hocking, G. C. & Vanden-Broeck, J.-M. 1996 Draining of a fluid of finite depth into a slot. *Appl. Math. Modeling* (submitted).

Larock, B. E. 1969 Gravity-affected flow from planar sluice gate. *ASCE J. Engng Mech. Div.* **96**, 1211–1226.

Vanden-Broeck, J.-M. 1980 Nonlinear stern waves. *J. Fluid Mech.* **96**, 601–610.

Vanden-Broeck, J.-M. 1986 Flow under a gate. *Phys. Fluids* **29**, 3148–3151.

Vanden-Broeck, J.-M. & Dias, F. 1992 Solitary waves in water of infinite depth and related free surface flows. *J. Fluid Mech.* **240**, 549–557.

Vanden-Broeck, J.-M. & Tuck, E. O. 1994 Steady inviscid rotational flows with free surfaces. *J. Fluid Mech.* **258**, 105–113.